

Invited paper

Strain directed assembly of nanoparticle arrays within a semiconductor

C.-Y. Hung¹, A.F. Marshall², D.-K. Kim¹, W.D. Nix³, J.S. Harris, Jr.¹ and R.A. Kiehl¹

¹*Solid State and Photonics Laboratory*, ²*Center for Materials Research*,

³*Department of Materials Science and Engineering, Stanford University, Stanford, CA 94305, USA*

Received 7 December 1998; accepted in revised form 15 April 1999

Key words: nanoparticles, self assembly, nanotechnology, precipitation, elastic properties

Abstract

The use of strain to direct the assembly of nanoparticle arrays in a semiconductor is investigated experimentally and theoretically. The process uses crystal strain produced by a surface structure and variations in layer composition to guide the formation of arsenic precipitates in a GaAs-based structure grown at low temperature by molecular beam epitaxy. Remarkable patterning effects, including the formation of single and double one-dimensional arrays with completely clear fields are achieved for particles in the 10-nm size regime at a depth of about 50 nm from the semiconductor surface. Experimental results on the time dependence of the strain patterning indicates that strain controls the late stage of the coarsening process, rather than the precipitate nucleation. Comparison of the observed particle distributions with theoretical calculations of the stress and strain distributions reveals that the precipitates form in regions of maximum strain energy, rather than near extremum points of hydrostatic stress or dilatation strain. It is therefore concluded that the patterning results from modulus differences between the particle and matrix materials rather than from other strain related effects. The results presented here should be useful for extending strain directed assembly to other materials systems and to other configurations of particles.

Introduction

A process for directing the assembly of nanoparticles within a solid so as to control the spatial distributions in one, two, or three dimensions is of potential interest for a variety of applications. The ability to precisely control the periodicity in particle arrays or the coupling between sets of particles could lead to materials with interesting optical or electronic properties. Moreover, if the positional control could be made to originate from structures that also provide electrical or optical access to the particles, this could open new possibilities for nanostructure devices and circuits.

Nanoparticles can be formed within a solid by the process of precipitation. The formation of nanocrystals within a semiconductor is of particular interest because this allows the electrical and optical properties of the

particle and the matrix to be tailored over wide ranges. In this paper we examine a process in which strain is used to direct the assembly of nanocrystals within a semiconductor by controlled precipitation (Kiehl et al., 1995, 1996; Hung et al., 1997, 1998). The process uses crystal strain and layer composition to guide the formation of arsenic precipitates in a GaAs-based structure grown at low temperature by molecular beam epitaxy (MBE). The inhomogeneous strain field produced by stressors fabricated on the surface of the epitaxial structure is used to control the lateral position of the particles, while the composition of the epitaxial layers controls the vertical position of the particles.

This paper is designed to be a comprehensive treatment of this topic in which essential background material and key prior results are briefly presented together with results from our recent experimental and

theoretical studies. We will begin by discussing the precipitation process for hexagonal arsenic crystals in non-stoichiometric GaAs grown at low temperatures by molecular beam epitaxy. The control of precipitate size and uniformity is discussed and the use of compositional variations to produce preferential precipitation in selected epitaxial layers is described. We then discuss results on strain directed assembly of one-dimensional particle arrays. Experimental results on the time dependence of the patterning effects during annealing are given first. Results on the observed dependence of the strain patterning on stressor geometry are presented next. The theoretical stress and strain distributions in our structure are then examined using the finite element method and compared with the observed particle distributions in the structures. As summarized in the conclusion of this paper, the theoretical and experimental results provide a detailed understanding of the patterning mechanism, which should be useful for extending this process to other materials systems and particle configurations.

Arsenic precipitation in non-stoichiometric GaAs

Growth of non-stoichiometric material

Molecular beam epitaxial growth of high-quality stoichiometric GaAs is typically done at a substrate temperature of 600°C, and an As/Ga flux ratio in the range of 15–20. If such a V/III flux ratio is maintained, but the substrate temperature is lowered to 200–250°C, the vapor pressure of As will be lower than the impinging As pressure and excess arsenic will tend to accumulate on the surface. As a result, as much as 1.5% excess As will be incorporated into the GaAs film, which is called non-stoichiometric (NS) or low-temperature-grown (LTG) GaAs (Melloch et al., 1992; Yu et al., 1992). Similar techniques can also be applied to grow NS-AlGaAs, NS-InGaAs and other non-stoichiometric arsenide layers.

The excess As incorporated into NS-GaAs results in various forms of point defects, such as arsenic anti-sites As_{Ga} , arsenic interstitials As_i and gallium vacancies V_{Ga} (Kaminska et al., 1989; Look et al., 1990), as shown schematically in Figure 1. The concentration of arsenic interstitials As_i appears to be negligible compared with As_{Ga} and V_{Ga} according to studies by Liu et al. (1995). Arsenic anti-site defects are found with concentrations in the range of 2×10^{19} to $1 \times 10^{20} \text{ cm}^{-3}$

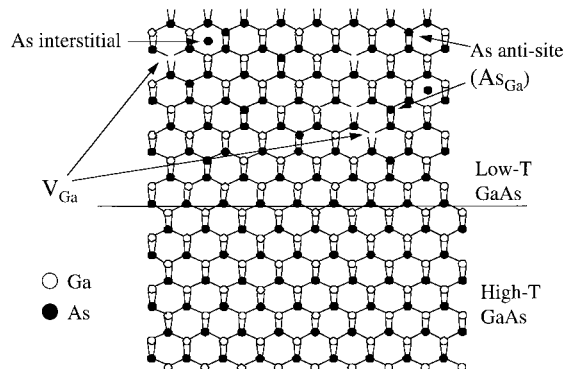


Figure 1. Schematic illustrating the point defects in arsenic rich non-stoichiometric GaAs prior to annealing. Non-stoichiometric GaAs is grown at low temperatures (e.g., 200°C) by molecular beam epitaxy.

in as-grown layers, depending on the growth temperature. The concentration of V_{Ga} in as-grown NS-GaAs is approximately 10^{19} cm^{-3} (Look et al., 1990).

The amount of excess arsenic incorporation is a strong function of the substrate temperature and increases as the growth temperature is decreased. The lattice constant of InGaAs is larger than that of GaAs because the As atom is larger than the Ga atom. As a result of this lattice mismatch, there is a limit to the amount of excess arsenic that can be incorporated into the layer by lowering the substrate temperature (Melloch et al., 1992). For a given amount of excess As, there will be a critical thickness beyond which the film turns polycrystalline or even amorphous.

Formation of arsenic precipitates during annealing

When NS-GaAs epilayers are annealed above about 400°C, the excess As atoms cluster to form precipitates (Melloch et al., 1992). A precipitation process is a solid–solid transformation and can be expressed as:

$$\alpha' = \beta + \alpha$$

where α' is the metastable supersaturated solid solution, β is a stable or metastable precipitate, and α is a more stable solid solution with the same crystal structure as α' but with a composition closer to equilibrium. In general, the approach to equilibrium for the supersaturated phase α' can occur by at least two mechanisms: (1) nucleation and growth and (2) spinodal decomposition. The precipitation of excess arsenic is believed to occur by nucleation and growth.

Nucleation occurs at the beginning of the precipitation process. The free energy difference between the α' matrix and the α' matrix with β -phase precipitates is the driving force for the nucleation of precipitates. In the nucleation of β -phase in a matrix of supersaturated α' -phase, B-atoms within the α' matrix must first diffuse together to form a small volume with the β composition. An interface must be created during this process and this also leads to a change in free energy. The total free energy change associated with the nucleation process will have three contributions

$$\Delta G_T = N^\beta(-\Delta g_a + \Delta g_{el}) + \eta\gamma(N^\beta)^{2/3}$$

where Δg_a is the difference in free energy per atom between the supersaturated α' -phase and the β -phase, Δg_{el} is the elastic strain energy per atom, γ is the interface free energy, and η is the shape factor. The elastic energy here results from a change in volume or shape during the precipitation process, which will be discussed in more detail later.

The first term in the above equation is usually negative, and the free energy of the system will decrease as B-atoms are added to the precipitate (a driving force for nucleation). However, the interfacial free energy and elastic energy will increase as the nucleus grows. Thus, if the total free energy change is plotted as a function of the nucleus radius, it will initially increase, reach a maximum point, and then decrease as the nucleus radius increases. The maximum (positive) change in the free energy in this transformation is called the 'nucleation barrier'.

The precipitate shape satisfying the above criterion is that which minimizes the total interfacial free energy. In the simplest case, the particles tend to have a spherical shape since this results in the minimum surface area for a fixed volume. This is the case of As precipitates in GaAs, the particles are observed to be nearly spherical.

Thus far, we have discussed the kinetics of an isolated precipitate and its surrounding matrix. If we now consider the situation with more than one precipitate in the matrix, one would expect that the growth of each precipitate will influence the others so as to minimize the total free energy of the whole system. This process is important in the late stages of precipitate growth, and is referred to as coarsening (Porter & Easterling, 1991). A high concentration of small precipitates will tend to coarsen into a lower concentration of large particles with a smaller total interfacial area in order to minimize surface energy. Coarsening dominated by surface energy in this way is known as 'Ostwald ripening' (Lifshitz & Slyozov, 1961).

In any two-phase system, including a matrix and precipitate, there will be a range of particle sizes due to differences in the time of nucleation and the rate of growth. In the case of two adjacent spherical precipitates with different diameters, the free energy per atom of the large precipitate is smaller than that of the small precipitate. According to the well known method of common tangents (Porter & Easterling, 1991), one finds that the solute (atom-B) concentration in the matrix adjacent to a particle is higher when the precipitate is smaller. Therefore, there will be a concentration gradient in the matrix which causes the solute (B atoms) to diffuse in the direction from the smaller particle toward the larger particle, so that the small particles shrink, and eventually disappear, while large particles grow. The overall result is that the total number of particles decreases and the mean radius increases with time.

Precipitate size and structure

Figure 2(a) and (b) are (110) cross-sectional transmission electron micrograph (TEM) images of As precipitates in GaAs samples annealed under different

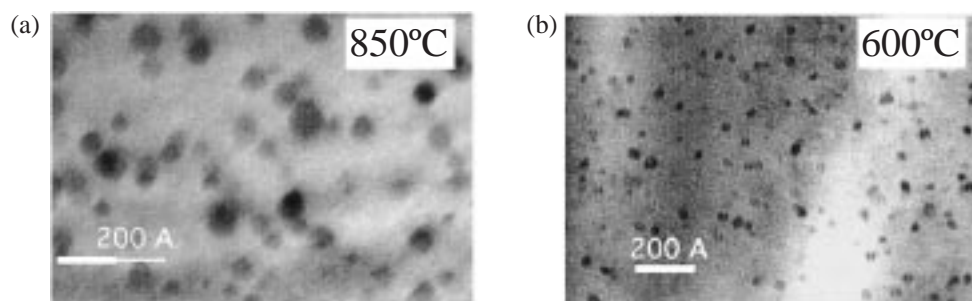


Figure 2. High resolution (110) cross-sectional TEM images, showing arsenic precipitates formed in GaAs after annealing at (a) 850°C (b) 600°C.

thermal cycles. At the lower anneal temperature the precipitates are small and very dense. At higher anneal temperatures, they are much larger and less dense, preserving the total arsenic volume.

The influence of the anneal temperature on the formation of As precipitates has been investigated by Melloch et al. using rapid thermal anneals (RTA) and furnace anneals (Melloch et al., 1992). Figure 3 summarizes the average sizes and spacings of precipitates as a function of temperature for a 30 s isochronal anneal for four different samples with various amounts of excess As in the range 0.2–0.9%. The data in Figure 3 shows that the size of the precipitates can be designed to be in the range of about 2–20 nm over this temperature range.

TEM images of large precipitates formed at 850°C and small precipitates formed at 600°C are shown in Figure 4. The images of the large precipitates show sets of lattice planes that are different from those of the surrounding GaAs, indicating a distinct crystal structure and that the lattices of the precipitate and the matrix are semicoherent (coherent in some directions and incoherent in others). In directions where the planes of the precipitate align with the matrix, misfit dislocations can sometimes be identified. The crystal structure of large precipitates has been determined to be hexagonal with (0003) planes oriented almost parallel to {111} planes of GaAs (Claverie & Weber, 1992). The image for the smaller precipitate in Figure 4 appears to be coherent with the surrounding GaAs. This is typical of what has been reported for As precipitates in the range of

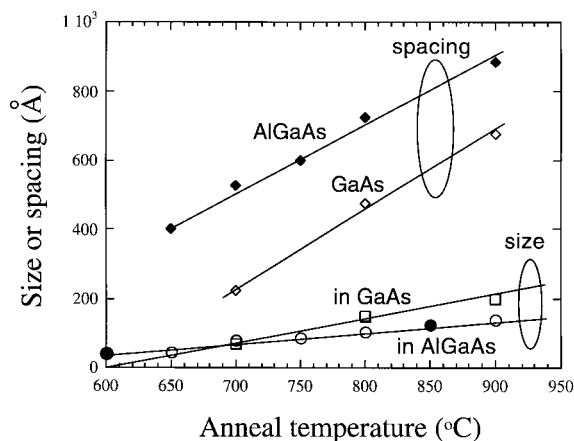


Figure 3. Average sizes and spacing of As precipitates in GaAs and AlGaAs as a function of the anneal temperature (After Melloch et al., 1992). The calibration samples from our experiments are shown as black circles.

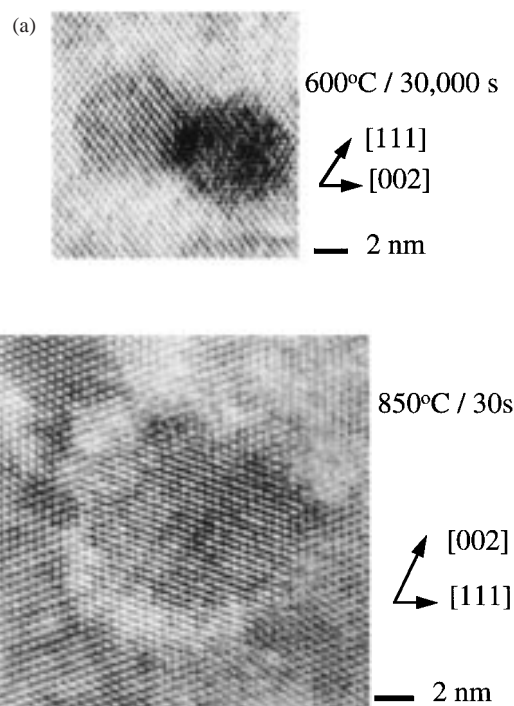


Figure 4. High resolution TEM image showing precipitates found in GaAs after annealing at (a) 600°C for 30,000 s and (b) 850°C for 30 s.

2–4 nm. The crystal structure of such small As precipitates, which has sometimes been referred to as 'pseudocubic' (Liliental-Weber et al., 1991), is not yet as well established.

Bulk hexagonal As is a semimetal and there is experimental evidence that As precipitates behave as buried metallic Schottky barriers (Mahalingam et al., 1992; Ibbetson et al., 1993). The electronic properties of semiconductor nanocrystals in the size regime where the particle contains only a few hundred or a few thousand atoms is strongly size dependent (Alivisatos, 1996), and some size dependence can also be expected in the case of semimetallic As precipitates. While the electronic properties are critical for potential nanoelectronic applications, this subject is beyond the scope of the present study, which is concerned with the patterning of the particles.

Preferential precipitation in heterostructure layers

In uniform layers of NS-GaAs, the precipitates nucleate homogeneously and are distributed uniformly in the

layers. In a NS-AlGaAs/GaAs heterostructure, however, precipitates form preferentially in the GaAs layers (Mahalingam et al., 1992). This effect has been attributed to the differences between the interfacial energies associated with the arsenic precipitates in the GaAs and the AlGaAs matrix. The interfacial energy of precipitates in GaAs is lower than in AlGaAs because the Ga-As bond is weaker than the Al-As bond. From this, one would expect a diffusion of As_{Ga} point defects from the AlGaAs layers to the GaAs layers so that the total free energy of the system is reduced, similar to Ostwald ripening. Thus, the preferential precipitation of As in GaAs is believed to be a coarsening process in which precipitates nucleate throughout the AlGaAs and GaAs layers but preferentially grow in the GaAs layers with continued annealing.

The above picture is supported by experiments on the time evolution of the precipitate distribution shown in Figure 5. The samples were annealed at 600°C for three different times. At this relatively low annealing temperature, the diffusion of atomic arsenic through the lattice is relatively slow and the buildup of particle density within the GaAs well can be clearly seen.

In NS-GaAs, a high concentration of vacancies (10^{19} cm^{-3}) exists in the as-grown layers. The presence of vacancies is important in the precipitation process since the diffusion of As_{Ga} anti-sites is vacancy assisted, as discussed by Bliss et al. (1992). During annealing, vacancies will diffuse to vacancy sinks, such as defect complexes or interfaces which include the sample surface, the layer interface, and the arsenic precipitate interface. Due to the annihilation of vacancies during annealing, the supersaturated vacancy density decreases with time. Therefore, there is a strong decrease in diffusion during annealing. Such details concerning the time dependence of the point defect concentrations are important to the preferential precipitation in epitaxial layers (Hung et al., 1998) and could also play a key role in the strain patterning effects of interest here.

Strain directed assembly of 1D nanoparticle arrays

Kiehl and coworkers (1995) were first to demonstrate that the lateral position of arsenic precipitates in GaAs can be controlled by a stress structure (stressor). Their original idea was based on the notion that an intentional modulation of strain in the epitaxial structure could be effective in determining the most favorable

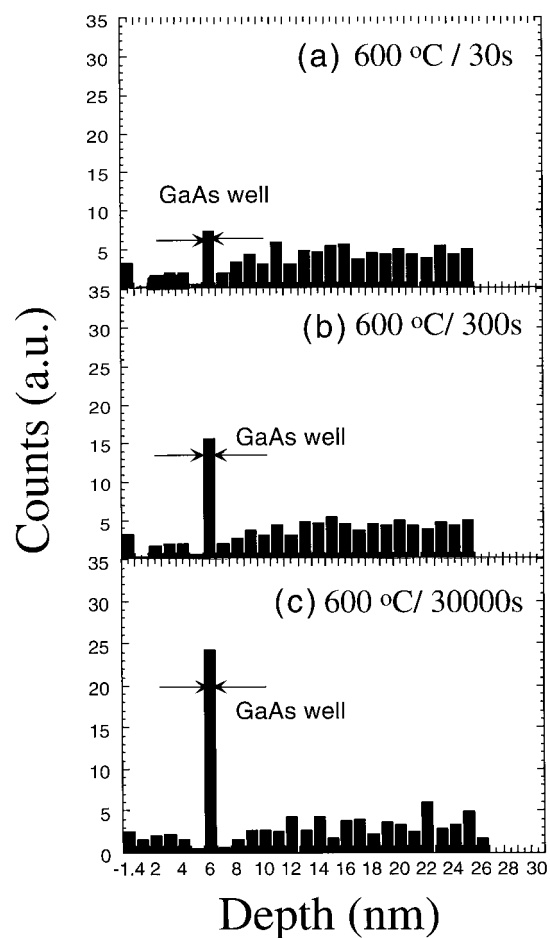


Figure 5. Histograms showing the distribution of arsenic precipitates in the growth direction for (a) 600°C/30 s, (b) 600°C/300 s, and (c) 600°C/30,000 s annealing cycles.

nucleation and equilibrium positions for arsenic precipitation in NS-GaAs. Initial experiments (Kiehl et al., 1995) showed a correlation between the position of near-surface precipitates in a homogeneous NS-GaAs structure and line stressors fabricated on the surface. Control of both the lateral and vertical positions of the precipitates was then demonstrated by combining strain patterning with preferential precipitation in an AlGaAs/GaAs heterostructure (Kiehl et al., 1996). Composition controls the vertical position of the particles, while strain controls the lateral position, as illustrated in Figure 6.

The structure used in these earlier experiments was based on a non-stoichiometric AlGaAs/GaAs/AlGaAs sandwich that was capped with a thin InGaAs-based layer. The GaAs and AlGaAs layers in the sandwich

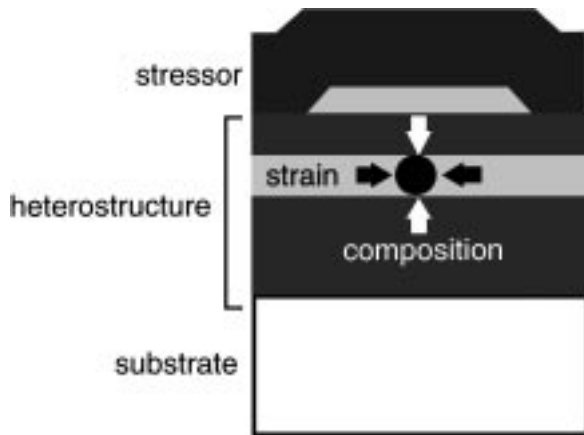


Figure 6. Schematic diagram illustrating the use of strain and composition to control the position of As precipitates in an AlGaAs/GaAs heterostructure.

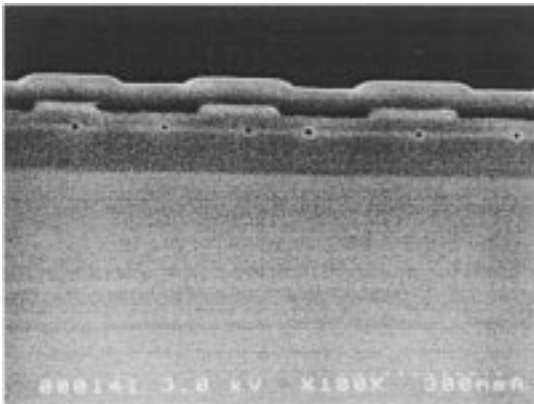


Figure 7. Cross-sectional SEM showing the strain directed assembly As precipitates in an AlGaAs/GaAs heterostructure with line stressors fabricated on the surface. The precipitate diameter and stressor width are approximately 20 and 200 nm, respectively. The precipitates have formed in a 10-nm GaAs layer (light-gray region). (After Kiehl et al., 1996).

were approximately 10 and 50 nm, respectively. The InGaAs layer in the structure is strained as a result of its larger lattice constant. After the growth of the sandwich, the InGaAs cap layer was patterned by e-beam lithography, covered by a SiN dielectric film, and annealed by rapid thermal annealing. The epitaxial structure, sample growth, and preparation procedures used in the present work are similar to those used in the earlier studies. Further details will be given later in this paper.

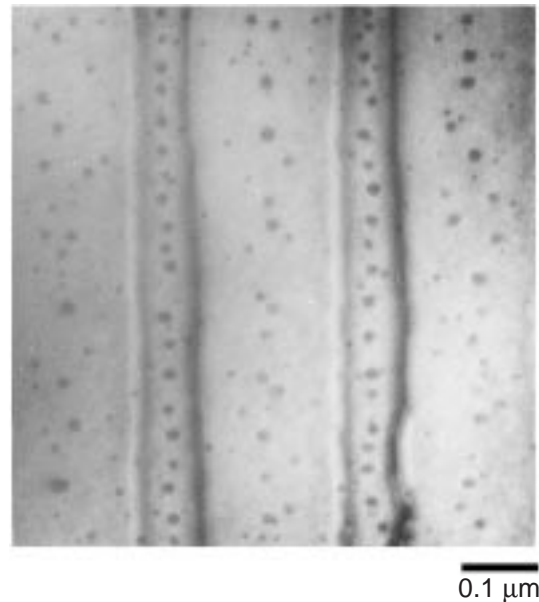


Figure 8. Plan view TEM showing the formation of 1D arsenic particle arrays beneath line stressors. The stressors are ~ 90 -nm wide and spaced with a 290-nm pitch. The particles beneath the stressors have an average diameter of 16 nm and an average edge-to-edge spacing of 23 nm. (After Kiehl et al., 1996).

Figure 7 shows a cross-sectional high resolution scanning electron micrograph (SEM) image of this type of sample after annealing. A single line of particles approximately 20 nm in diameter can be seen centered under each stressor. Particles are also found in the spaces between the stressors. The particles are vertically positioned at the plane of the GaAs layer (the light gray band in the image) at a depth of 45 nm from the etched AlGaAs surface.

In order to observe the distribution of particles along the stressor lines, the samples were also examined by plan-view (TEM). A plan-view TEM micrograph is shown in Figure 8 for a sample having approximately 90-nm wide stressor lines set at a 290-nm pitch. It is seen that 1D arrays of particles with an average diameter of 16 nm and average edge-to-edge spacing of 23 nm are formed beneath the stressors.

The above results show that the particles (1) form in a single line beneath each stressor, (2) form a dispersed distribution centered midway between stressors, and (3) are almost completely absent within wide bands running along each stressor edge.

Time and geometry dependencies of strain patterning

Materials growth and sample preparation

In order to investigate the extent of the strain patterning and to gain a better understanding of the detailed mechanism behind this effect, we examined the dependencies of the patterning on annealing cycle and the stressor geometry. The samples were grown in a Varian GEN II MBE system on a two-inch diameter substrate. The growth rates were typically $0.15 \mu\text{m/h}$ and $0.27 \mu\text{m/h}$ for GaAs and AlGaAs, respectively, with a ratio of group V to group III beam equivalent pressures equal to 36.

A 200 nm GaAs buffer layer was first grown on a semi-insulating substrate to eliminate defects from the substrate. This was followed by a 50-nm $\text{Al}_{0.4}\text{Ga}_{0.6}\text{As}$ layer, which serves as a blocking layer for the diffusion of excess arsenic from the upper layers. These first two layers were stoichiometric layers grown at 600°C . The substrate temperature was then lowered to 200°C and three non-stoichiometric layers were grown: 200 nm

of $\text{NS-Al}_{0.4}\text{Ga}_{0.6}\text{As}$, 10 nm of NS-GaAs, and 50 nm of $\text{NS-Al}_{0.4}\text{Ga}_{0.6}\text{As}$. Finally, the substrate temperature was raised to 450°C and the following layers were grown: 2 nm of GaAs, 12 nm of $\text{In}_{0.3}\text{Ga}_{0.7}\text{As}$, and a 4 nm GaAs cap.

The top three layers of the structure are used in the fabrication of surface stressors. InGaAs has a larger lattice constant than GaAs, with a lattice mismatch of 7.1% for pure InAs. When grown epitaxially on GaAs, the InGaAs lattice strains to match the in-plane lattice constant of the underlying GaAs substrate. Strained layers that are free of misfit dislocations can be grown, provided that the layer is below a composition dependent critical thickness.

Surface stressors consisting of narrow lines formed in the strained top layers of the structure were fabricated by patterning the surface by e-beam lithography and etching through to the $\text{NS-Al}_{0.4}\text{Ga}_{0.6}\text{As}$ layer with a selective wet chemical etch. To prevent arsenic loss through the surface during the anneals, a Si_3N_4 dielectric film was then deposited by plasma enhanced chemical vapor deposition at 350°C . Different annealing temperatures were employed in an ambient of

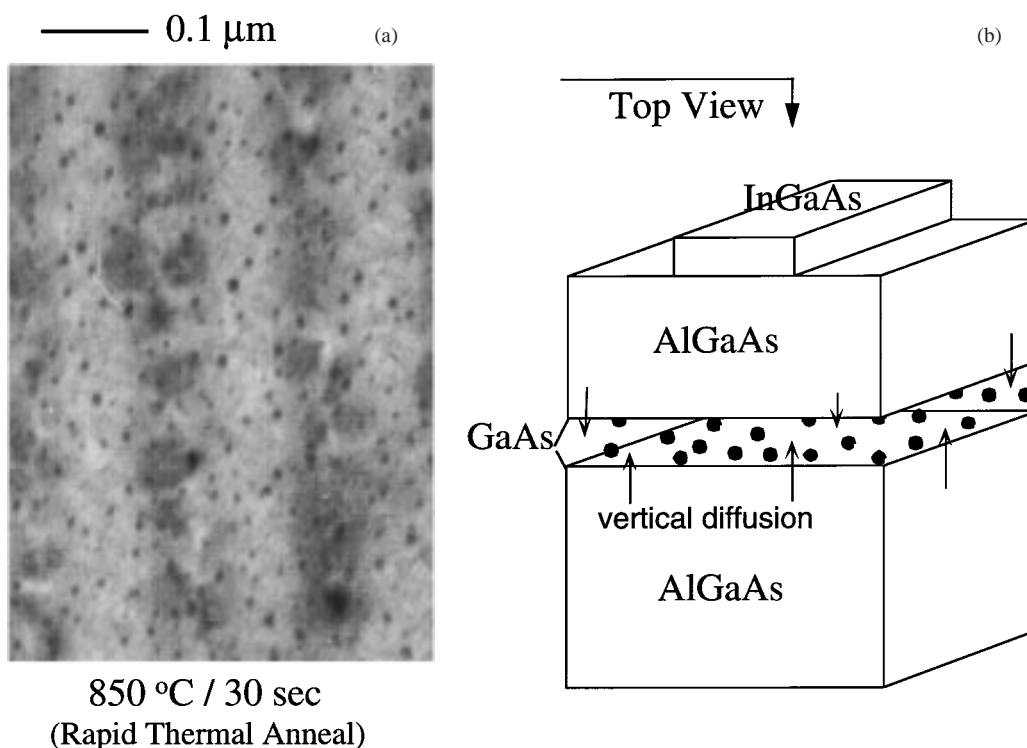


Figure 9. Plan-view TEM image and schematic illustrating the patterning for a $850^\circ\text{C}/30 \text{ s}$ anneal.

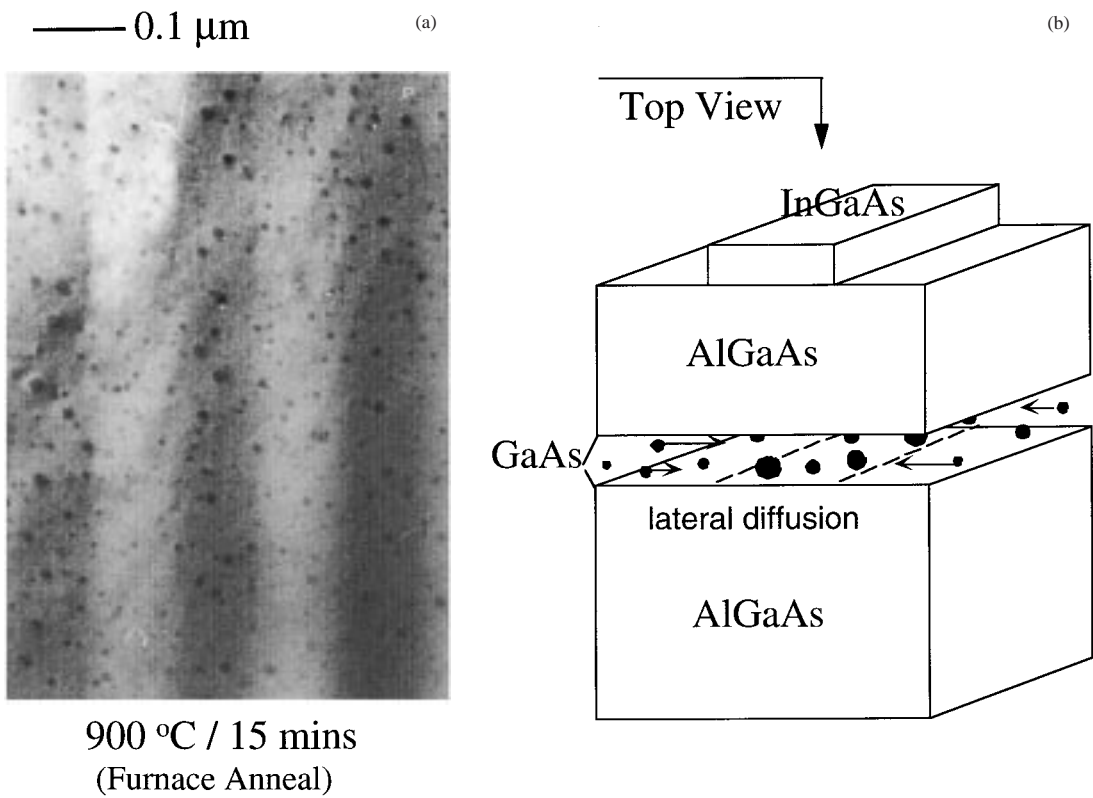


Figure 10. Plan-view TEM image and schematic illustrating the patterning for a 900°C/15 min anneal.

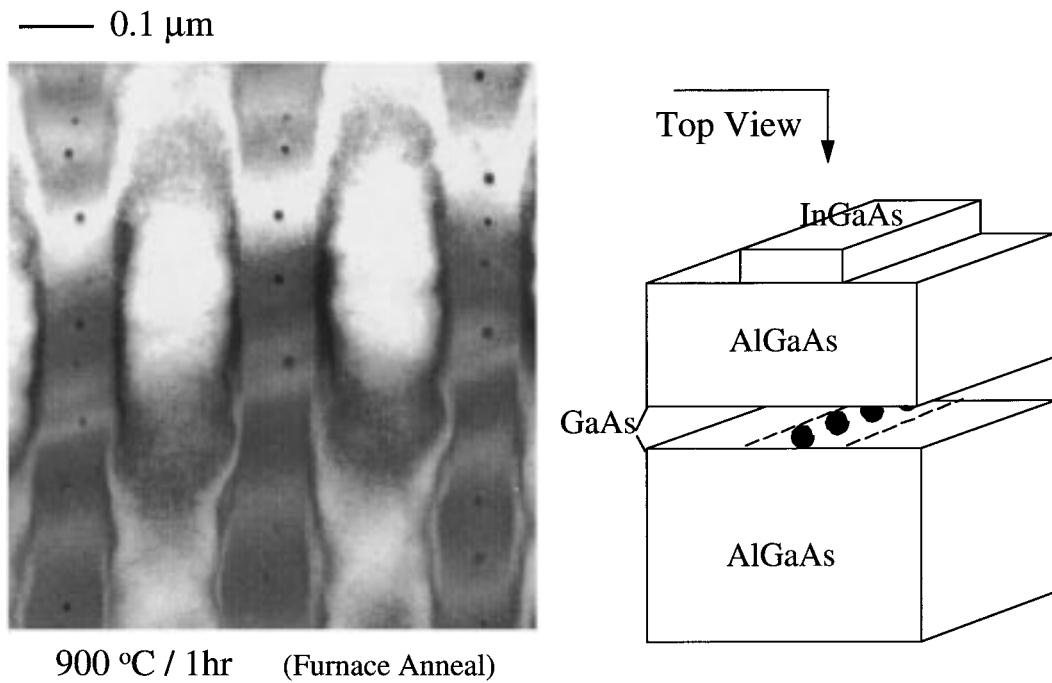


Figure 11. Plan-view TEM image and schematic illustrating the patterning for a 900°C/1 h anneal.

nitrogen and forming gas for three different anneal times, 30, 300 and 30,000 s. Rapid thermal annealing (RTA) was used for the two shorter anneals and a furnace (quartz tube) anneal was used for the longest anneal. The distributions and sizes of arsenic precipitates in the structure were examined by TEM in $\langle 110 \rangle$ cross section.

Time dependence

Figures 9, 10, and 11 are the bright-field plan-view TEM micrographs under the (001) zone-axis condition, showing the lateral distributions of arsenic precipitates along the InGaAs stressor lines in the annealed samples for the three annealing cycles. The main variable in this set of experiments is the annealing time.

Figure 9(a), the annealing case of 850°C/30 s, shows that arsenic precipitates were uniformly distributed across the sample with no evidence of strain patterning. Cross-sectional TEM analysis of this sample showed that a preferential coarsening of arsenic precipitates had occurred in the NS-GaAs layer so that most of the precipitates were confined in this plane although they were not strain patterned laterally, as illustrated in the Figure 9(b).

When the anneal time was increased to 15 min, a noticeable strain patterning appeared. Figure 10 shows a higher precipitate density beneath the InGaAs stressors. Close inspection of the micrographs indicated that the particle density beneath the stressors was higher than in the spaces by a factor of about 2.4. We also observed that the arsenic precipitates underneath the stressors are larger than those in between. These results show that the strain patterning involves the diffusion of excess arsenic from the spaces to the region beneath the stressors, as illustrated in Figure 10(b). Figure 11 presents the case of the longest anneal, one hour. The arch-shaped contrast and wide dark bands around and across the InGaAs stressor lines are diffraction contrast from the bending of the thin TEM specimen. Note that, because of this influence, some arsenic particles were either hidden or showed a gray contrast in the darker regions. Three interesting results are shown in this image: (1) a single line of arsenic particles with an average size of 14.4 nm beneath each InGaAs stressor, (2) a field clear of arsenic particles in the spacing region between the stressors, and (3) a more uniform particle spacing (90 nm in average) underneath the stressors compared to those seen in Figures 9 and 10.

The formation of a single line of precipitates with completely clear fields shown in Figure 11 is quite dramatic. Moreover, the trend in the results of Figures 9 through 11 provide information that is useful in determining the details of the strain patterning mechanism. One possible scenario has been that strain modulates the nucleation barrier, so that precipitates nucleate earlier beneath the stressor. These larger particles would tend to grow faster than the smaller particles in the spaces, as in the case of normal Ostwald ripening. Our results show, however, that the size distribution of particles in the early stage of growth is uniform with no noticeable spatial dependence. Thus, it appears that the effect of strain on the nucleation barrier does not play an important role in the patterning. Instead, it appears

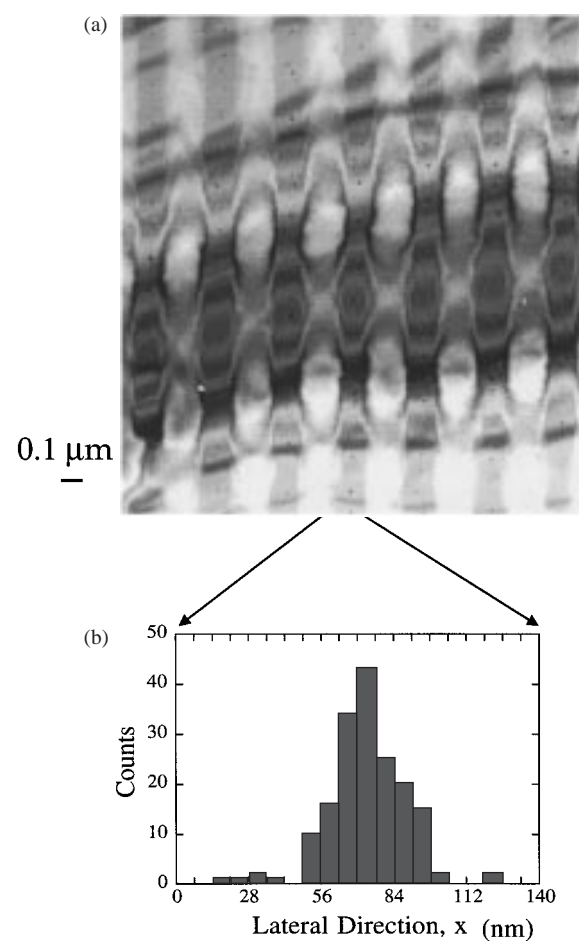


Figure 12. (a) Plan-view TEM image and (b) histogram of the arsenic distribution beneath the stressors for a sample with 135 nm stressors. The annealing cycle was 900°C for 1 h.

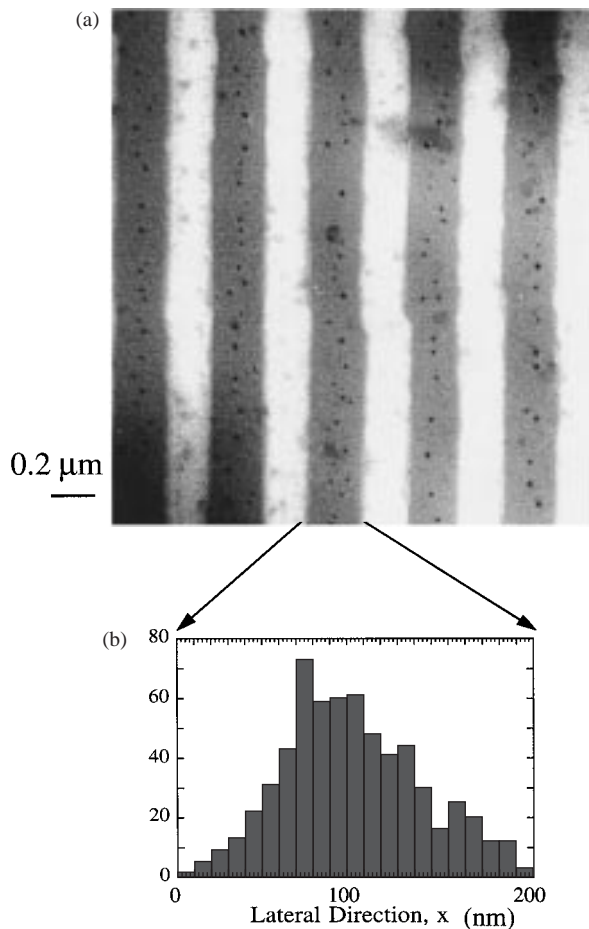


Figure 13. (a) Plan-view TEM image and (b) histogram of the arsenic distribution beneath the stressors for a sample with 200 nm stressors. The annealing cycle was 900°C for 40 min.

that the strain patterning is a coarsening effect, similar to what is observed for preferential precipitation due to composition. In other words, rather than controlling the position where particles initially form, the strain modulates the redistribution of atomic arsenic between the precipitates during the late stages of coarsening. As a result, the arsenic particles beneath the InGaAs stressor grow while others shrink and eventually disappear.

Geometry dependence

We have also experimentally examined the dependence of the strain patterning on the width of the stressor. Figure 12 shows a plan-view TEM image for the same

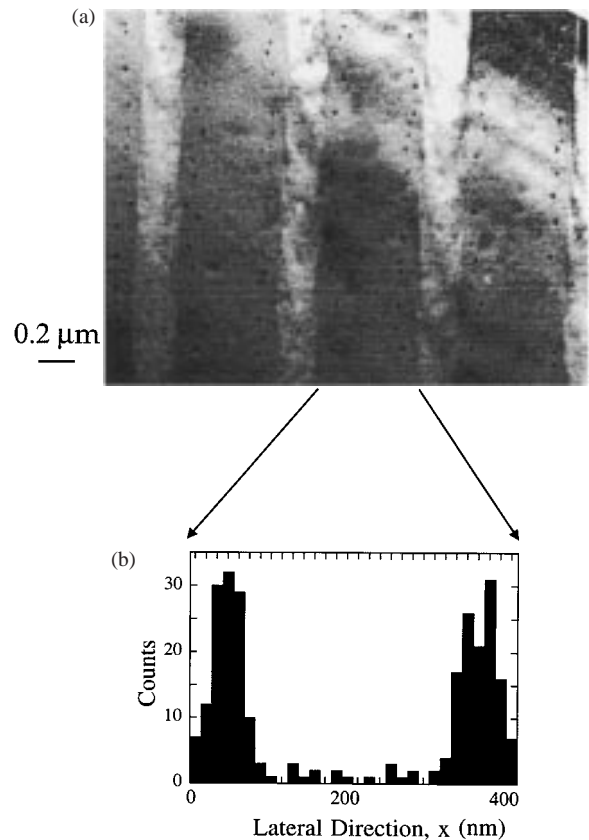


Figure 14. (a) Plan-view TEM image and (b) histogram of the arsenic distribution beneath the stressors for a sample with 410 nm stressors. The annealing cycle was 900°C for 40 min.

sample as in Figure 11, but over a larger area. The width of the stressors in this case is 135 nm. A histogram showing the lateral distribution of precipitates beneath the stressors is shown in Figure 12(b). The distribution is sharply peaked in the middle of the stressor. (Note that the extent of the horizontal axis in the histogram corresponds to the stressor width.)

Figure 13 shows the plan-view TEM image and histogram for a wider stressor having a width of 200 nm. In this case we observe that precipitates deviate from the middle point of the stressor, i.e., the distribution broadens. Figure 14 shows the TEM image and histogram for a 410 nm wide stressor. At a width of 410 nm, arsenic precipitates no longer form along the center line of the stressor. Instead, they form in narrow regions just inside of the two edges of the stressor, thereby forming a double-line array of particles. We will discuss this dependence of the distribution on stressor geometry in the next section.

Stress and strain calculation

In order to gain a better understanding of the detailed mechanism of the strain patterning observed in our experiments, an analysis was made of the stress and strain fields in our structure, which is shown schematically in Figure 15. The sources of strain are (1) the epitaxial mismatch strain between InGaAs and GaAs layers, (2) the thermal strain during annealing due to different thermal expansion coefficients among InGaAs, GaAs, AlGaAs, and Si₃N₄, and (3) the strain produced by the stress in the dielectric cap on the patterned semiconductor structure. The various parameters include the composition of the InGaAs layer, the width (w) and thickness (t) of the stressor, and the composition and thickness of the dielectric cap.

The origins of strain in a thin film grown on a substrate usually include thermal strain, intrinsic strain and epitaxial strain (Baker & Nix, 1990). These three strains are described by:

$$\text{Thermal : } \varepsilon_{\text{misfit}} = (\alpha_f - \alpha_s)(T - T_0)$$

$$\text{Intrinsic : } \varepsilon_{\text{misfit}} = \Delta_{\text{transformation}}/3$$

$$\text{Epitaxial : } \varepsilon_{\text{misfit}} = (d_f - d_s)/d_s$$

where T_0 is the growth temperature, α is the thermal expansion coefficient of the material, and d is the

lattice constant of the material. $\Delta_{\text{transformation}}$ is the volume change of a thin film if a phase transformation occurs during the thermal cycle, the subscript 'f' indicates 'thin film', and 's' stands for 'substrate'.

The coefficients of thermal expansion and lattice constants of GaAs, AlAs, InAs and SiN were taken from the literature (Neuberger, 1971; Walle, 1989), assuming a linear relationship with composition in the alloy systems. This gives an epitaxial strain between the In_{0.25}Ga_{0.75}As and Al_{0.4}Ga_{0.6}As layers used in our structure equal to 0.0176. The thermal strains between the In_{0.25}Ga_{0.75}As, Al_{0.4}Ga_{0.6}As, GaAs and Si₃N₄ layers are usually two or three orders of magnitude lower than the epitaxial strain, even for temperatures several hundred of degrees away from the growth or deposition temperature.

We are interested in the stress and strain distributions in the AlGaAs/GaAs/AlGaAs epitaxial layers where the precipitates form. The InGaAs layer and Si₃N₄ cap can be considered as surface features producing the stress and strain. The rest of the structure is taken to be a non-rigid GaAs substrate since the mechanical properties of AlGaAs and GaAs are nearly the same. A general purpose finite element code, MARC (1988), was used to solve the strains/stresses for the geometry involved. Because this code cannot directly model the epitaxial strain, an effective thermal mismatch was used to

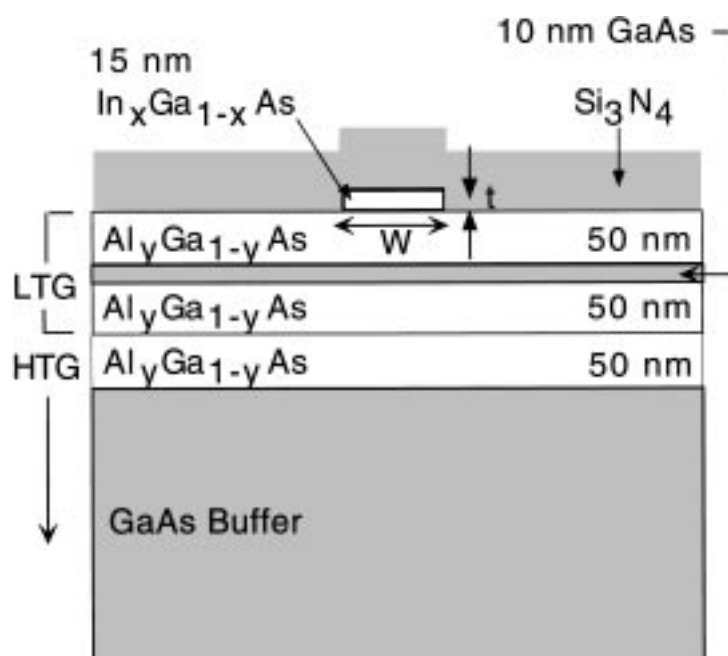


Figure 15. Schematic showing the geometry of the patterned epitaxial structure with the Si₃N₄ dielectric cap.

approximate the epitaxial strain (Xu & Petroff, 1991). This was done by using an effective coefficient of thermal expansion (CTE) for the InGaAs layer, based on the layer mismatch and the annealing temperature. The same method was used to model the stress conditions of the Si_3N_4 films.

Figure 16 shows a diagram of the geometry used in the simulation, including boundary conditions. The thickness of the Si_3N_4 passivation over the stressor is the same over the stressor and the substrate. The stressor, the dielectric, and the substrate are assumed to be perfectly bonded. The structure is constrained so that it is not displaced in the x -direction at the nodes along the y -axis, as indicated in the figure. Moreover, the substrate is assumed to be much larger than the stressor in each direction and constrained not to move in either the x or the y directions at the lower left node. Since our stressors are very long compared to their width and height, the boundary conditions of the plane strain case

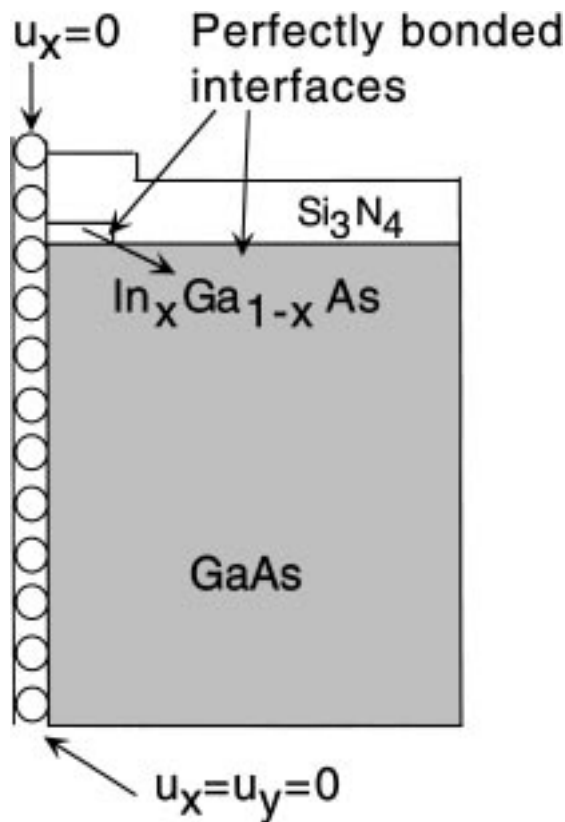


Figure 16. Geometry and boundary conditions for the structure modeled in the finite element method calculations.

are used to reduce the situation to the two dimensional case.

Figure 17 shows the two-dimensional contour plots of the FEM results for the strain distributions in the case of a stressor thickness t and width w equal to 15 and 100 nm, respectively. The Si_3N_4 layer was taken as 70 nm. These values are close to the experimental values for the narrow stressor. Figure 17(a), (b) and (c) show the ϵ_{xx} , ϵ_{yy} , and ϵ_{xy} fields, respectively. The rectangular block of concentrated contours in Figure 17(a) shows the position of the InGaAs stressor. The region to the right and above this block is the Si_3N_4 dielectric (which follows the contour of the patterned semiconductor) and the region below the block represents the epitaxial AlGaAs/GaAs layers and a portion of the GaAs substrate. Figure 17(a) shows that the InGaAs stressor is under compression in the x -direction. The patterning of the InGaAs layer allows the strain to relax at its edges, thereby generating a tensile strain field in the x -direction beneath the stressor. Figure 17(b) shows that the strain field beneath the stressor is compressive in the y -direction as a result of the Poisson effect. Figure 17(c) shows a large shear strain is generated at the edges of the stressor.

The experimental results described earlier in this paper indicate that the particle distribution builds up in the buried GaAs layer due to compositional differences prior to the effect of strain patterning. Thus, the strain and stress distributions within the GaAs layer centered 50 nm below the surface should be the most important for the strain patterning. In Figures 18 and 19, we compare the calculated components of the strain and stress fields at a depth corresponding to the center of the GaAs layer for two different stressor widths, representing the narrowest and widest stressors examined in the experiments.

Figure 18 shows results for a stressor width w equal to 100 nm. In this case, a transverse tensile strain ϵ_{xx} and a normal compressive strain ϵ_{yy} are produced in the GaAs well mainly by the strain relaxation at the edge of the stressor. These components have extremum values beneath the center of the InGaAs stressor. The shear strain, ϵ_{xy} is positive and its maximum appears underneath the edge of the stressor. The dilatation strain, Φ , which is defined by the sum ϵ_{xx} , ϵ_{yy} and ϵ_{zz} , is plotted in the same figure as well. Figure 18(b) is the stress plot for the same stressor geometry. Each component of the stress shows a trend similar to its corresponding strain. σ_{xx} in the GaAs well has a maximum value of 0.15 GPa

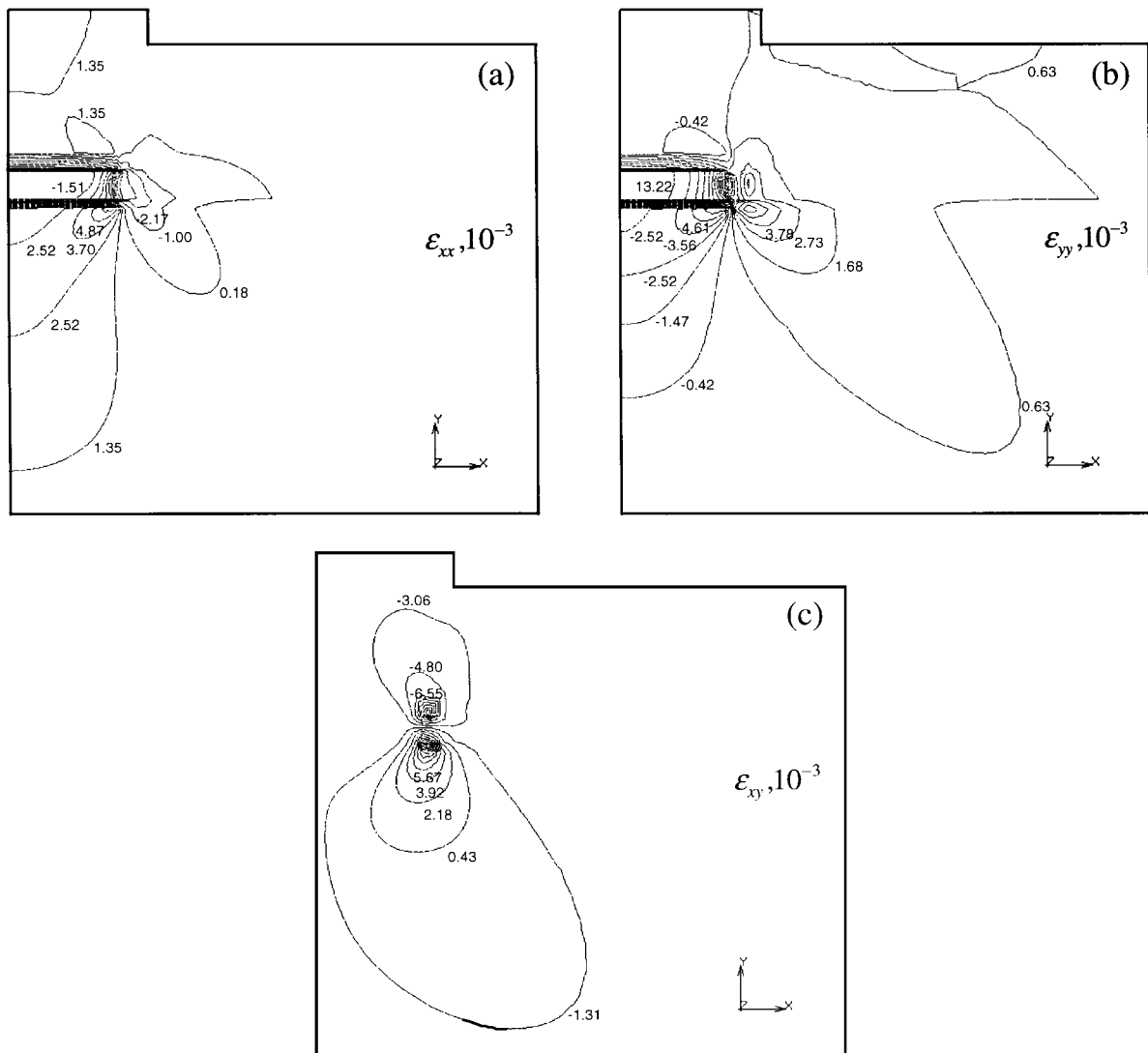


Figure 17. Two-dimensional contour plots of the FEM results for transverse strain ϵ_{xx} , normal strain ϵ_{yy} , and shear strain ϵ_{xy} .

in tension. This is about one-tenth of the biaxial stress in a uniform $\text{In}_{0.25}\text{Ga}_{0.75}\text{As}$ film on a GaAs substrate. The hydrostatic stress, ΔT , which is equal to the sum $1/3(\sigma_{xx} + \sigma_{yy} + \sigma_{zz})$, is also shown. Note that neither the dilatation strain nor the hydrostatic stress exhibit a strongly peaked behavior and that the values of these components beneath the stressors are comparable to those between the stressors.

The calculated strain and stress distributions at the depth of the GaAs layer are plotted in Figure 19 for a large stressor width of 500 nm. The ϵ_{xx} and ϵ_{yy}

values beneath the stressor are tensile and compressive, respectively, as seen in the previous case of the narrow stressor. However, the peak positions of both strain components shift from the center to a position just inside the edge of the stressor. The shear strain is zero at the center and goes through negative values before reaching its maximum at the edge of the stressor. Note that the dilatation strain and hydrostatic stress distributions are again relatively flat and take on comparable values beneath and outside of the stressor.

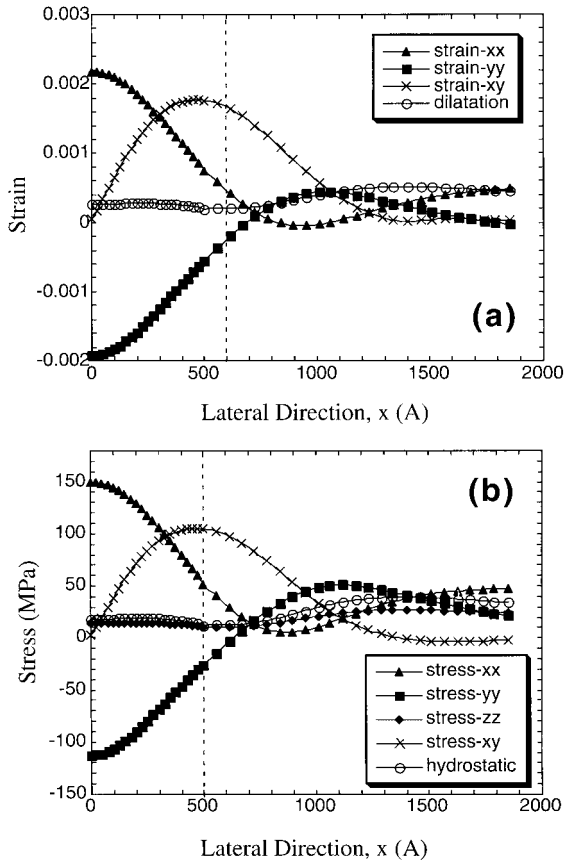


Figure 18. The (a) strain and (b) stress fields in the NS-GaAs layer along the x -direction for $t = 15$ nm, $w = 100$ nm, and a tensile Si_3N_4 cap.

Strain patterning mechanism

A reduction of elastic energy can be the driving force for the migration of excess arsenic in an inhomogeneous strain field. The reduction in the free energy of the whole system can come from three sources: changes in particle shape due to diffusion, volume changes of particles under stress, and modulus differences between the particle and matrix materials. We examine these in the following.

Effects due to particle shape

When a precipitate is under a non-uniform stress field or the applied stresses at the interface between the precipitate and the matrix are not symmetrical, the precipitate is loaded with a stress state, which includes a pure shear stress. This situation is illustrated in Figure 20(a). The

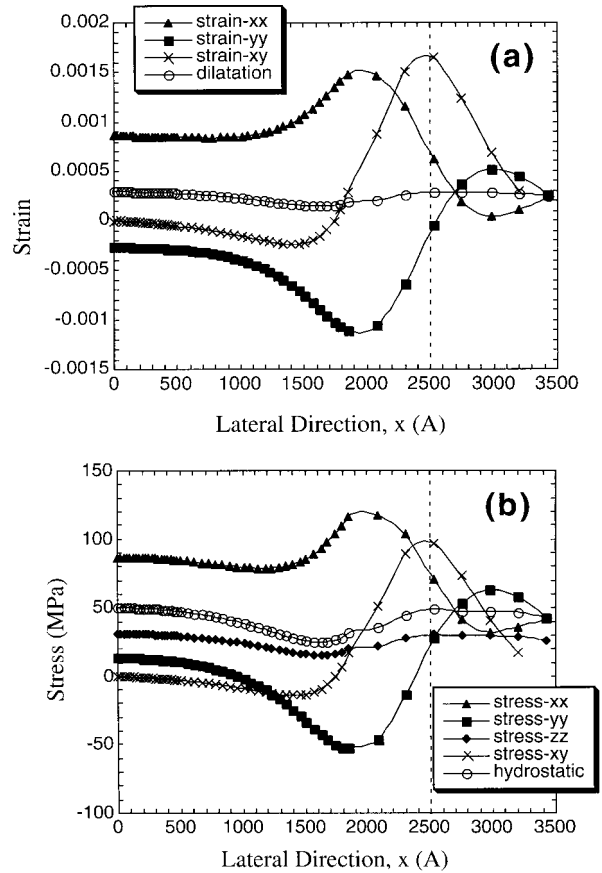


Figure 19. The (a) strain and (b) stress fields in the NS-GaAs layer along the x -direction for the same parameters as in Figure 18, except $w = 500$ nm.

presence of the shear will create normal traction on the surface of the precipitate such that two diametrically opposed points on the sphere are positions of maximum compression, and perpendicular to this diameter are two diametrically opposed points which are centers of maximum tension. As a result, the shape of the precipitate can change from a sphere to an ellipsoid with an elongation in the original direction of maximum tension until the stresses at the interface become symmetric, as shown in Figure 20(a).

The diffusion relaxation of the shear is accompanied by a decrease in the elastic interaction energy, which is usually proportional to the square of the shear stress. However, the magnitude of this effect is usually much smaller than those from the effects of size and modulus change. Moreover, the migration of the solute atoms in this case usually occurs locally in each precipitate, not among the precipitates. Thus while this effect might

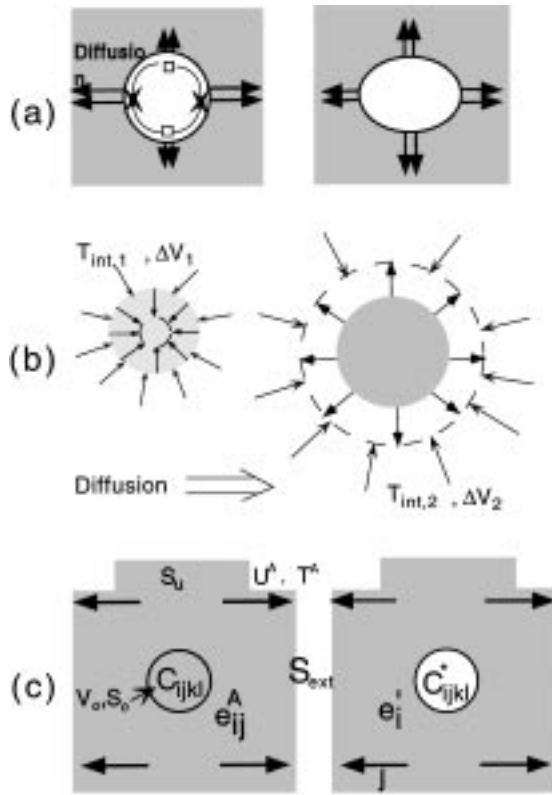


Figure 20. Schematic showing the effect of (a) diffusion, (b) volume change, and (c) shear modulus differences on the elastic interaction.

lead to a slight modulation in the shape of precipitates in our structure, it is unlikely that this effect plays an important role in the strain patterning.

Effects due to volume differences

If we regard the precipitates as elastic spheres, the energy of a precipitate in a crystal can be considered as the strain energy created in the system by the expansion or contraction of a cluster of solvent atoms to a size equal to that of the same number of solute atoms. In the present case, the excess arsenic atoms are considered as the solute and the GaAs matrix as the solvent. The strain energy of an arsenic precipitate in the GaAs matrix can be simply estimated within this picture if we consider that the formation of an As precipitate is accomplished by replacing Ga atoms originally located in this volume with As atoms. For the case of a stress-free medium, this strain energy is due entirely to the elastic resistance of the material (GaAs) surrounding

the (As) precipitate. However, if the expansion (or contraction) occurs in a region already subjected to a stress (strain) field, extra work will be done against the forces acting on the precipitate from this field. This will alter the total strain energy of the system by an amount that is called the energy of interaction of the precipitate and the stress field.

When the stress field is non-uniform, the work done by expanding a precipitate against the field will vary with the position of the precipitate in the field. Because all systems have a tendency to decrease their free energy (the strain energy in this case), atoms in the precipitate will experience a force driving them to the region where the precipitates can have a lower interaction energy. The volume of each precipitate changes correspondingly.

Figure 20(b) is a schematic diagram showing the changes in volume among particles. The variation of the interaction energy due to the volume change is given by

$$\Delta U_{int}^{volume}(x_i, y_i, z_i) = (-T_{int} \Delta V)_i = (-T_{int} \cdot V \cdot \Theta)_i$$

where T_{int} is the hydrostatic stress, Θ is the dilatation and V is the original volume of the precipitate formed by the solutes. We see that this quantity depends upon the dilatation and the hydrostatic stress in the neighborhood of the precipitate.

The finite element calculations show that the spatial dependence of the dilatation and hydrostatic stress are about the same for the wide and narrow stressor geometries. Thus, the trends in these quantities cannot explain why the precipitates form a single-line array beneath a narrow stressor and double-line array beneath a wide stressor, and it is clear that the strain patterning does not correspond to a minimization of the energy of interaction related to the volume differences between the hexagonal As and GaAs crystals.

Effects due to modulus differences

The atoms in the precipitates and the atoms in the matrix may have the same size but different stiffnesses, one being elastically softer than the other. The interaction energy is also affected by the difference between the stiffnesses of the materials (Fleischer, 1961). Such an elastic non-uniformity interacts with the stress field. Under a uniform stress field, an additional interaction energy will be generated and added to the total elastic energy of the whole system. If the stress field is non-uniform, the interaction energy of each particle will vary with its position in the field. Thus, there will be

a force driving the migration of solute atoms between precipitates so as to reduce the total elastic energy with the result that some precipitates grow while others shrink.

Figure 20(c) is a schematic diagram showing the effect of modulus change on the elastic interaction. Consider a homogenous, finite, linear elastic solid whose external boundary S_{ext} is subjected to given displacements U^A (strains) and given tractions T^A (stresses) on the portion of S_{ext} denoted as S_0 . Now imagine that a volume V_0 with bounding surface S_0 has its elastic stiffnesses changed from their original constant values C_{ijkl} to new constant values given by C_{ijkl}^* while the original boundary conditions on S_{ext} are maintained, as illustrated in Figure 20(c). The change of the interaction energy produced by this modulus difference is given by

$$\begin{aligned} \Delta U_{\text{int}}^{\text{modulus}}(x_i, y_i, z_i) &= 1/2(C_{ijkl}^* - C_{ijkl}) \\ &\times \int_{V_{0,i}} e_{ij}^A e'_{kl} dV \end{aligned}$$

where e_{ij}^A and e'_{ij} represent the strain states before and after the elastic constants are changed.

In the present case of hexagonal-As and cubic GaAs, the particle and matrix have very different elastic constants. GaAs has a zinc-blend structure with stiffness coefficients $C_{11} = 118$ GPa, $C_{12} = 53$ GPa and $C_{44} = 59$ GPa; arsenic has a hexagonal structure with the stiffness coefficients $C_{11} = 130$ GPa, $C_{33} = 58.7$ GPa, $C_{44} = 22.5$ GPa, $C_{12} = 30.3$ GPa, $C_{13} = 64.3$ GPa and $C_{14} = -3.7$ GPa. Comparing C_{44} for the two materials, we see that hexagonal-As is elastically softer than GaAs. Therefore, the effect of modulus differences on the elastic interaction could play an important role in the relaxation of elastic strain energy in our case. In the following section, we examine this possibility.

It should be mentioned that the As precipitate and GaAs matrix lattices are semicoherent in the particle size regime of these experiments, as discussed earlier. However, even in the case of incoherent particles, the relaxation of strain will, in general, depend on the relative elastic properties of the particle and matrix. Only in the special case of pure shear strain can the relaxation be independent of the elastic properties of the particle. In the general case, where there are hydrostatic components to the strain state (as seen in Figure 19), the relative elastic properties will play a role even if the interfaces can freely slide and allow easy diffusion.

Strain energy distributions

To examine the effect of modulus difference on strain patterning, we make two simplifying approximations. First, the GaAs substrate and arsenic precipitates are taken to be elastically isotropic materials. Second, since the difference in the strains before and after the modulus change are generally very small, we assume $e'_{ij} = e_{ij}^A$. Thus, the above equation can be simplified to be (Timoshenko & Goodier, 1970)

$$\begin{aligned} \Delta U_{\text{int}}^{\text{modulus}}(x_i, y_i, z_i) &= 1/2(E^* - E) \int_{V_{0,i}} e_{ij}^A e_{kl}^A dV \\ &= 1/2\Delta E \sum_{jk} \varepsilon_{jk}^2 \\ &= 1/2 \frac{\Delta E}{E} E \sum_{jk} \varepsilon_{jk}^2 \\ &\quad (j \text{ or } k = x, y, z) \\ &= f U_i \end{aligned}$$

where E^* and E are the Young's modulus of arsenic and GaAs, respectively, since the stiffness in any direction is equal to the Young's modulus for an isotropic material. The ε_{jk} are the components of the strain tensor and U_i is the strain energy originally stored in the system, such as that induced by the stressors, and is given by

$$U_i = \sum_{jk} 1/2 E \varepsilon_{jk}^2.$$

The factor f represents the ratio of the modulus difference to Young's modulus of GaAs. Since arsenic is elastically softer than GaAs and most of its stiffness coefficients C_{ijkl} are smaller than those of GaAs, $E^* - E$ and, in turn, the factor f have negative values in our case. Since the strain energy is always positive, we know from the equations above that the change of modulus from $E(\text{GaAs})$ to $E^*(\text{As})$ in the volume of V_0 results in a reduction of the interaction energy (or the total elastic energy of the system). This will be a force driving the migration of excess arsenic as discussed above.

The importance of the above is that it shows that the change in the interaction energy that occurs when a particle is introduced at a given position is simply proportional to the original strain energy at that position. The interaction energy is reduced when the particle is softer than the lattice. Thus, due to the modulus differences for our materials, the arsenic precipitates should tend to grow at positions of larger strain energy, since this will reduce the total free energy for the whole system.

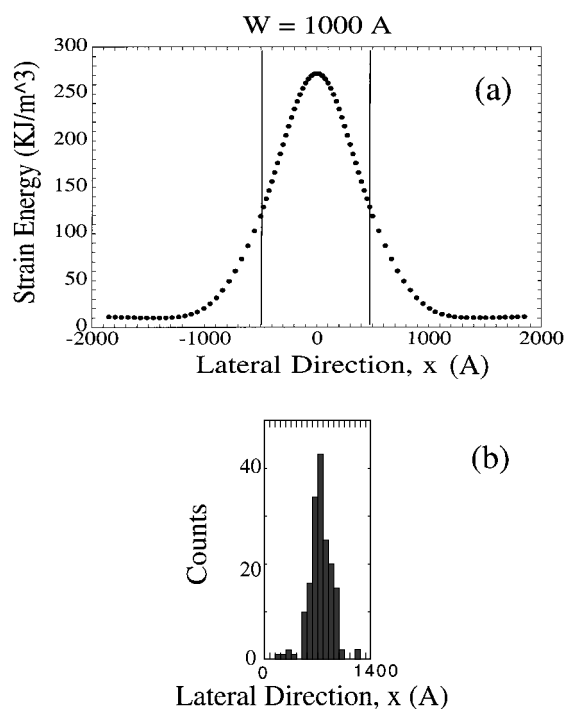


Figure 21. Comparison of (a) the calculated strain energy distribution and (b) the experimental particle distribution for a 100 nm wide stressor. The strain energy at the depth of the confining GaAs layer (the particle plane).

Plots of the calculated strain energy in the GaAs layer are shown for a narrow stressor in Figure 21 and a wide stressor in Figure 22. Histograms of the experimental particle distributions for narrow and wide stressors are also shown in the figures. It can be seen that the experimental particle distributions are in excellent agreement with the peaks in the calculated strain energy plots. Therefore, we conclude that the reduction in strain energy related to the difference between the modulus of the As precipitates and the GaAs matrix is responsible for the strain patterning observed in our experiments.

From the above, one can roughly explain the trends in the lateral patterning effects of the precipitates observed in our experiments as follows. The inhomogeneous strain fields in the epitaxial AlGaAs/GaAs layers are mainly caused by the strain relaxation at the edges of the InGaAs stressors. When the stressor is very wide, the strain is maximum near its edges and small near its center. As the width of the stressor decreases, the peak of strain moves towards the center from both

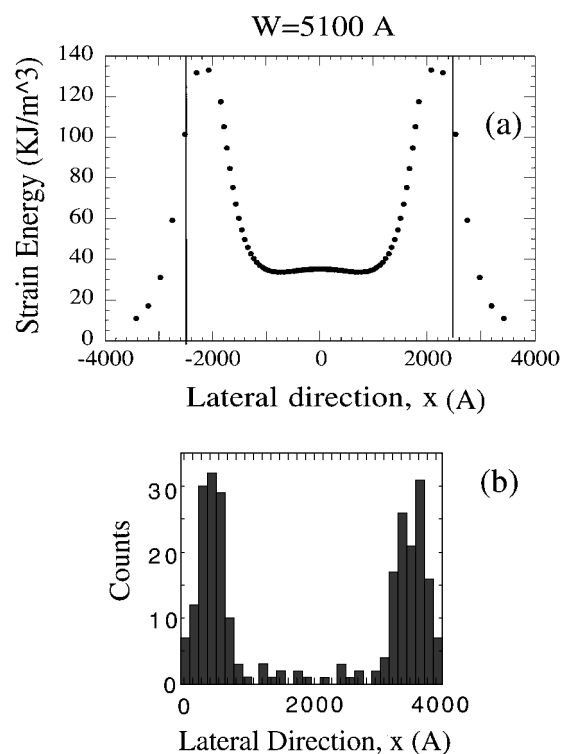


Figure 22. Comparison of (a) the calculated strain energy distribution and (b) the experimental particle distribution for a 410 nm wide stressor. The strain energy at the depth of the confining GaAs layer (the particle plane).

edges, finally merging and becoming a single peak at the center.

To exploit the strain patterning effect, the stressor should be designed to produce a maximum in strain energy at the desired particle position. In structures such as ours where layer composition is used to control the vertical position of the particles, it is the strain energy in the plane where the particles will be confined that is most important. In the simple case where it is desired to form particles in a single line beneath the stressor, narrowing the stressor leads to a single peak in the strain energy distribution. However, since the penetration depth of the strain field decreases in proportion to the stressor width, narrowing the stressor reduces the strain at a given depth. Thus there is an optimum width for strain patterning. This is illustrated in Figure 23, which shows the calculated strain energy in the confining GaAs layer as a function of stressor width.

Strain energy calculations such as those described here should be useful for designing stressors for assembling other configurations of particles. For example,

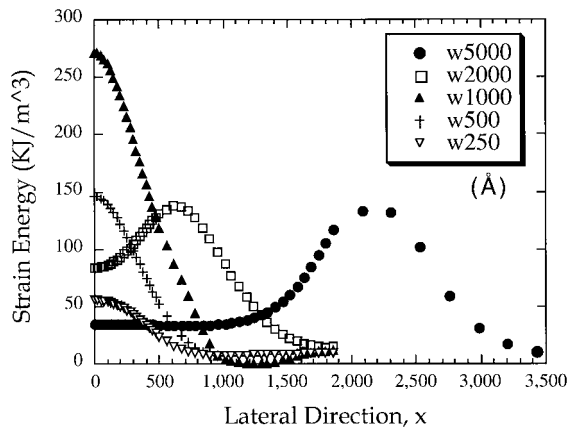


Figure 23. Calculated strain energy distribution for various stressor widths. (The width w is shown in Å.)

designs optimized for strain release at the corners of a square or polygon-shaped stressor could be used to fabricate assemblies of closely spaced particles in nearly arbitrary configurations.

Conclusion

The use of strain to direct the assembly of nanoparticle arrays in a semiconductor was investigated experimentally and theoretically in this paper. Remarkable patterning effects, including the formation of single and double one-dimensional arrays with completely clear fields were achieved for 10-nm particles at a depth of 50 nm from the surface. Experimental results on the time dependence of the strain patterning indicate that strain controls the late stage of the coarsening process, rather than the precipitate nucleation stage. Comparison of the observed spatial particle distributions with theoretical calculations of the stress and strain distributions in the structure reveals that the precipitates form in regions of maximum strain energy, rather than near extremum points of hydrostatic stress or dilatation strain. Based on these results, we conclude that the patterning results from modulus differences between the particle and matrix materials, rather than from volume differences or other strain related effects. Thus, it is the relative softness of the As precipitates compared to the GaAs matrix that is the key to the strain patterning observed in our experiments.

The results presented here should be useful for extending strain directed assembly to other materials systems and to other configurations of particles.

An important feature of this process is that, in addition to providing a means for assembling arrays and arbitrary configurations of particles, strain patterning also provides a means for self-aligning particles to an optical or electrical access structure, since this structure could be the stressor itself. Thus, strain directed assembly could provide an attractive high throughput fabrication technology for nanoelectronic circuits and other applications. One interesting example is single-electron tunneling circuitry (Likharev, 1999), which is based on electron tunneling in assemblies of conductive nanometer-scale particles.

Acknowledgements

The authors would like to acknowledge technical contributions from T. Cuk. R. A. Kiehl would also like to thank his coworkers at Fujitsu Laboratories, who collaborated in the early experiments on this topic. This work was supported by the Air Force through contract F49620-97-1-0444 and by ONR/DARPA through contract N00014-96-1-0983. Support from Fujitsu Laboratories, Ltd. is also gratefully acknowledged.

References

- Alivisatos A.P., 1996. Perspectives on the physical chemistry of semiconductor nanocrystals. *J. Phys. Chem.* 100, 13226–13239.
- Baker S.P. & W.D. Nix, 1990. Mechanical properties of thin films on substrates. *SPIE Optical Thin Films III: New Developments*, 263.
- Bliss D.E., W. Walukiewicz, I.J.W. Ager, E.E. Haller, K.T. Chan & S. Tanigawa, 1992. Annealing studies of low-temperature-grown GaAs:Be. *J. Appl. Phys.* 71, 1699.
- Claverie A. & Z. Liliental-Weber, 1992. Structure and orientation of As precipitates in GaAs grown at low temperature by molecular beam epitaxy. *Philos. Mag.* A 65, 981.
- Fleischer R.L., 1961. Solution hardening. *Acta Metallurgica* 9(11), 996.
- Hung C.-Y., J.S. Harris, A.F. Marshall & R.A. Kiehl, 1997. Arsenic Precipitation in GaAs for Single-electron Tunneling Applications. *Intl. Symp. Compound Semiconductors*, San Diego, Calif.
- Hung C.-Y., J.S. Harris, A.F. Marshall & R.A. Kiehl, 1998. Annealing cycle dependence of preferential arsenic precipitation in AlGaAs/GaAs layers. *Appl. Phys. Lett.* 73(3), 330–332.
- Ibbetson J.P., J.S. Speck, N.X. Nguyen & A.C. Gossard, 1993. The role of microstructure in the electrical properties of GaAs grown at low temperature. *J. Electronic Materials* 22, 1421–1424.

- Kaminska M., Z. Liliental-Weber, E.R. Weber, T. George, J.B. Kortright, F.W. Smith, B.Y. Tsaur & A.R. Calawa, 1989. Structural properties of As-rich GaAs grown by molecular beam epitaxy at low temperatures. *Appl. Phys. Lett.* 54, 1881.
- Kiehl R.A., M. Saito, M. Yamaguchi, O. Ueda & N. Yokoyama, 1995. Lateral patterning of arsenic precipitates in GaAs by a surface stress structure. *Appl. Phys. Lett.* 66, 2194.
- Kiehl R.A., M. Yamaguchi, O. Ueda, N. Horiguchi & N. Yokoyama, 1996. Patterned self-assembly of one-dimensional arsenic particle arrays in GaAs by controlled precipitation. *Appl. Phys. Lett.* 68(4), 478–480.
- Lifshitz I.M. & V.V. Slyozov, 1961. *J. Phys. Chem. Solids* 19, 35.
- Likharev K.K., 1999. Single-electron devices and their applications. *Proc. IEEE* 87(April), 633–651.
- Liliental-Weber Z., G. Cooper, J.R. Mariella & C. Kocot, 1991. The role of As in molecular-beam epitaxy GaAs layers grown at low temperature. *J. Vac. Sci. Technol. B* 9, 2323.
- Liu X., A. Prasad, J. Nishio, E.R. Weber, Z. Liliental-Weber & W. Walukiewicz, 1995. Native point defects in low-temperature-grown GaAs. *Appl. Phys. Lett.* 67, 279.
- Look D.C., D.C. Walters, M.O. Manasreh, J.R. Sizelove, C.E. Stutz & K.R. Evans, 1990. Anomalous Hall-effect results in low-temperature molecular beam epitaxial GaAs: hopping in a dense EL2-like band. *Phys. Rev. B* 42, 3578.
- Mahalingam K., N. Otsuka, M.R. Melloch, J.M. Woodall & A.C. Warren, 1992. Arsenic precipitate accumulation and depletion zones at AlGaAs/GaAs heterojunctions grown at low substrate temperature by molecular beam epitaxy. *J. Vac. Sci. Technol. B* 10, 812.
- MARC, 1988. MARC finite element program. Palo Alto, CA, MARC Analysis Research Corporation.
- Melloch M.R., N. Otsuka, K. Mahalingam, A.C. Warren, J.M. Woodall & P.D. Kirchner, 1992. Incorporation of excess arsenic in GaAs and AlGaAs epilayers grown at low substrate temperatures by molecular beam epitaxy. *Mater. Res. Soc. Sym. Proc.* 241, 113.
- Neuberger M., 1971. *Handbook of Electronic Materials*, IFI/Plenum Data Corporation.
- Porter D.A. & K.E. Easterling, 1991. *Phase Transformation in Metals and Alloys*, Chapman and Hall, International Publications.
- Timoshenko S.P. & J.N. Goodier, 1970. *Theory of Elasticity*, McGraw-Hill Book Company.
- Walle C.G. V.d., 1989. Band lineups and deformation potentials in the model-solid theory. *Phys. Rev. B* 39, 1871.
- Xu Z. & P.M. Petroff, 1991. Strain-induced carrier confinement in a buried stressor structure. *J. Appl. Phys.* 69, 6564.
- Yu K.M., M. Kaminska & Z. Liliental-Weber, 1992. Characterization of GaAs layers grown by low temperature molecular beam epitaxy using ion beam techniques. *J. Appl. Phys.* 72, 2850.